See page 1006

Engineering Liver-detargeted AAV9 Vectors for Cardiac and Musculoskeletal Gene Transfer

Nagesh Pulicherla[1], Shen Shen[1,2], Swati Yadav[1], Kari Debbink[1], Lakshmanan Govindasamy[3], Mavis Agbandje-McKenna[3] and Aravind Asokan[1,2,4]

[1]Gene Therapy Center, University of North Carolina at Chapel Hill, Chapel Hill, North Carolina, USA; [2]Molecular and Cellular Biophysics Program, University of North Carolina at Chapel Hill, Chapel Hill, North Carolina, USA; [3]Department of Biochemistry and Molecular Biology, Center for Structural Biology, McKnight Brain Institute, University of Florida, Gainesville, Florida, USA; [4]Department of Genetics, University of North Carolina at Chapel Hill, Chapel Hill, North Carolina, USA

We report the generation of a new class of adeno-associated virus serotype 9 (AAV9)-derived vectors displaying selective loss of liver tropism and demonstrating potential for cardiac and musculoskeletal gene transfer applications. Random mutagenesis of residues within a surface-exposed region of the major AAV9 capsid protein yielded a capsid library with mutations clustered at the icosahedral threefold symmetry axis. Using a combination of sequence analysis, structural models, and *in vivo* screening, we identified several functionally diverse AAV9 variants. The latter were classified into three functional subgroups, with respect to parental AAV9 displaying: (i) decreased transduction efficiency across multiple tissues; (ii) a selective decrease in liver transduction, or (iii) a similar transduction profile. Notably, variants 9.45 and 9.61 (subgroup II) displayed 10- to 25-fold lower gene transfer efficiency in liver, while transducing cardiac and skeletal muscle as efficiently as AAV9. These results were further corroborated by quantitation of vector genome copies and histological analysis of reporter (tdTomato) gene expression. The study highlights the feasibility of generating AAV vectors with selectively ablated tissue tropism, which when combined with other targeting strategies could allow sharply segregated gene expression. Liver-detargeted AAV9 variants described herein are excellent candidates for preclinical evaluation in animal models of cardiac and musculoskeletal disease.

Received 12 November 2010; accepted 26 January 2011; published online 1 March 2011. doi:10.1038/mt.2011.22

INTRODUCTION

Clinical gene transfer with adeno-associated viral (AAV) vectors has rapidly gained momentum in recent years. The ongoing translation from bench-to-bedside has been spurred in part by the availability of a versatile AAV toolkit displaying diverse tissue tropisms across multiple species.[1,2] Among numerous AAV isolates, AAV9 vectors display a systemic, multiorgan transduction profile following intravenous administration.[3] Rapid onset of gene expression and high transgene expression levels mediated by AAV9 vectors in heart and liver have been reported.[4–6] In addition, efficient transduction of neurons in neonatal mice as well as skeletal muscle in neonatal dogs following intravascular administration has been observed.[7,8] These attributes make AAV9 a viable candidate for therapeutic gene transfer in systemic diseases such as lysosomal storage disorders.

Paradoxically, a wide range of clinically relevant applications require vector targeting to specific tissues rather than multiorgan gene expression. For instance, gene therapy of cardiac disease or muscular dystrophies requires vectors capable of efficient and selective gene transfer to heart and/or skeletal muscle.[6,8,9] Therapeutic approaches targeting the liver or skeletal muscle are preferred for treatment of hemophilic disorders,[10] while the lung is considered a target organ for gene therapy of α-1 antitrypsin deficiency.[11,12] Tissue-specific transgene expression has been achieved through different approaches. For instance, at the vector genome level, transcriptional targeting elements such as tissue-specific promoters[13,14] and microRNA-mediated gene regulation[15] have been developed. When used in conjunction with the appropriate AAV serotype or variant, the latter strategies can provide exquisite control over gene expression patterns in different tissues following systemic injection.

Attempts to develop tissue-targeted AAV vectors have included insertion of targeting motifs into the GH loop of VP3 subunits of different AAV capsid templates or directed evolution of tissue-tropic AAV variants through DNA shuffling.[16–19] These efforts, in conjunction with alanine scanning mutagenesis studies have been instrumental in implicating the icosahedral threefold symmetry axis of AAV as a key determinant in the recognition of host cell surface receptors.[2,20–22] This highly variable trimer region, formed by interdigitation of GH loops from three VP3 subunits is thought to influence diverse tissue tropisms displayed by different AAV strains.[23–27] The current study hinges on re-engineering GH loop residues on the AAV9 capsid surface. Using a combination of sequence analysis, structural models, and *in vivo* screening, we identified several functionally diverse AAV9 capsid variants. Specifically, we report the discovery of novel AAV9 variants displaying attenuated liver

Correspondence: *Aravind Asokan, CB # 7352, Gene Therapy Center, 4101 Thurston Building, The University of North Carolina at Chapel Hill, Chapel Hill, North Carolina 27599-7352, USA. E-mail: aravind@med.unc.edu*

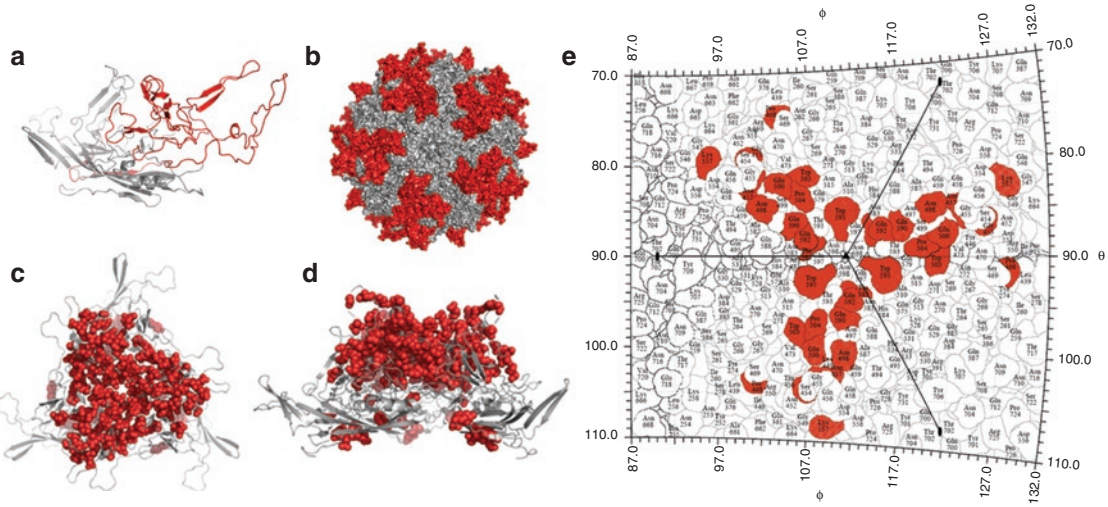

Figure 1 Structural analysis of the adeno-associated virus serotype 9 (AAV9) capsid library. (**a**) Cartoon representation of the AAV9 VP3 subunit monomer obtained using SWISS-MODEL with crystal structure of AAV8 serving as template (pdb id: 2QA0). The GH loop containing amino acids 390–627 (VP1 numbering) is colored in red. (**b**) Surface rendering of an AAV9 capsid model with 60 VP3 subunits generated using $T = 1$ icosahedral symmetry coordinates on VIPERdb. GH loop regions from different VP3 subunits, surrounding the icosahedral fivefold pore and interdigitating at the threefold symmetry axis are highlighted in red. (**c**) Cartoon of AAV9 VP3 subunit trimer generated on VIPERdb with point mutations of 43 representative clones from the AAV9 library depicted by red spheres. (**d**) Side view of capsid trimer (90° rotation) showing a majority of point mutations (red spheres) clustered on the outer loops. (**e**) Spherical roadmap projection of surface residues within the capsid trimer region. Residues highlighted in red represent a subset of ten AAV9 variants containing altered residues prominently located on the capsid surface.

tropism and with significant potential for therapeutic gene transfer in the treatment of musculoskeletal and cardiac diseases.

RESULTS

Structural models reveal mutations clustered within the AAV9 VP3 trimer

Using error-prone PCR, we generated a diverse AAV9 capsid library with focused mutations on the GH loop spanning amino acids 390-627 (VP1 numbering). A total of 96 variants were sequenced, following which 43 viable clones were obtained (**Supplementary Table S1**). Variants with stop codons, frame shift mutations, deletions/insertions were triaged. The variable loop region subjected to mutagenesis is highlighted in red in a model of the VP3 subunit and VP3 trimer of AAV9 (**Figure 1a,b**). Mapping of individual amino acid changes (red spheres) pertaining to each of the 43 different clones onto an AAV9 trimer model revealed clustering of mutations predominantly on the outer surface of VP3 (**Figure 1c,d**). Following this visualization, amino acid changes within β-strands and other regions that are highly conserved among different AAV strains were eliminated from further analysis. Lastly, a schematic "roadmap" projection of the AAV9 capsid model was generated to map the location of surface-exposed mutations (**Figure 1e**). Through this combination of sequence analysis and structural analysis, a subset of ten structurally diverse AAV9 surface variants (**Table 1**) were selected for vector production and characterization *in vivo*.

AAV9 variants display two distinct systemic transduction profiles

Ten AAV9 variants packaging the chicken β-actin (CBA) promoter-driven firefly luciferase transgene were generated at titers within two- to threefold that of parental AAV9 vectors. Bioluminescent images of mice injected through the tail vein with different AAV9 variants (5×10^{10} vg/animal) were obtained at 4 weeks postadministration. A qualitative analysis of transduction patterns revealed two distinct profiles, i.e., altered or unaltered when compared to parental AAV9 vectors (**Figure 2a,b**). First, as seen in **Figure 2a**, variant AAV9.11 appears to be a transduction-deficient variant. Marked changes in transduction profiles along with decreased transduction efficiencies in the liver region are also observed for variants 9.24, 9.45, 9.47, and 9.61. In addition, variant AAV9.68 appears to display a transduction profile favoring the liver. Secondly, as seen in **Figure 2b**, variants 9.9, 9.13, 9.16, and 9.84 display transduction profiles that remain largely unaltered compared to AAV9 vectors.

Transgene expression and biodistribution studies reveal three different functional phenotypes

Luciferase activities and vector genome copy numbers in tissue lysates were analyzed to compare transduction efficiencies of AAV9 and the variants in major organs including brain, heart, lung, liver, and skeletal muscle. Consistent with previous reports, AAV9 displayed robust transduction in heart, liver, skeletal muscle, and modest transgene expression levels in brain and lung.[3,4,6] In comparison, several variants displayed transduction efficiencies that ranged from several orders of magnitude lower than AAV9 within the liver to ~1 log unit lower in heart and skeletal muscle (**Figure 3a**). A similar trend was noted when comparing the vector genome copy numbers of variants with parental AAV9 in liver, with modest decrease in vector genome copies (fivefold or lower) within other tissues (**Figure 3b**). We then assigned each individual variant to a specific functional subtype on the basis of their corresponding transduction efficiency and biodistribution profile as detailed below.

Table 1 Summary of AAV9 variants characterized in this study

Variant	Point mutations	Functional subtype
9.9	W595C	II/III
9.11	T568P, Q590L	I
9.13	N457H, T574S	III
9.16	Q592L	II/III
9.24	W503R	II
9.45	N498Y, L602F	II
9.47	S414N, G453D, K557E, T582I	I
9.61	N498I	II
9.68	P504T	III
9.84	P468T, E500D	II/III

Abbreviations: I, transduction-deficient; II, liver-detargeted; III, similar to AAV9.

Functional subtype I. Variants displaying a defective phenotype were assigned to functional subtype I (black bars, **Figure 3a,b**). First, AAV9.11 displayed a significant decrease in transduction efficiency across multiple organs ranging from fivefold (lung) to 500-fold (liver). For this variant, decrease in vector genome copy numbers within respective tissue types was disproportionate, ranging from no significant change in skeletal muscle to ~1 log unit within the liver. Thus, in agreement with image analysis, AAV9.11 appears to be transduction-deficient. Variant AAV9.47 displays defective transduction levels ranging from threefold (heart) and sevenfold (skeletal muscle) to 110-fold (liver). A concomitant decrease in vector genome copy numbers (~4- to 140-fold) is seen in respective tissues. These results support the notion that AAV9.47 might display a defective biodistribution profile, which in turn adversely affects transduction efficiency. Taken together, the aforementioned results suggest that AAV9.11 and 9.47 constitute the functionally defective subtype I.

Functional subtype II. Variants significantly deficient in liver transduction, but showing modest-to-no change (approximately twofold or lesser) in other tissue types were assigned to functional subtype II (white bars, **Figure 3a,b**). Specifically, variants 9.24, 9.45, and 9.61 displayed ~10- to 25-fold decrease in transduction levels within the liver. A corresponding decrease in vector genome copy numbers ranging from ~10- to 25-fold is also observed within the liver. The AAV9.24 variant displayed a modest, yet significant decrease (approximately twofold) in transgene expression levels within the heart and brain. No marked changes in vector genome copy numbers within tissue types other than the liver were observed. Thus, variants 9.24, 9.45, and 9.61 were categorized as liver-detargeted AAV9 variants under the functional subtype II.

Functional subtype III. Variants displaying transduction profile and biodistribution largely similar to AAV9 in multiple tissue types were assigned to functional subtype III (gray bars, **Figure 3a,b**). Specifically, AAV9.13 and 9.68 displayed a modest increase (approximately three- to fivefold) in transduction efficiency as well as vector genome copy number within different tissue types. Interestingly, AAV9.68 displayed a slightly increased propensity for liver transduction in comparison with AAV9 and

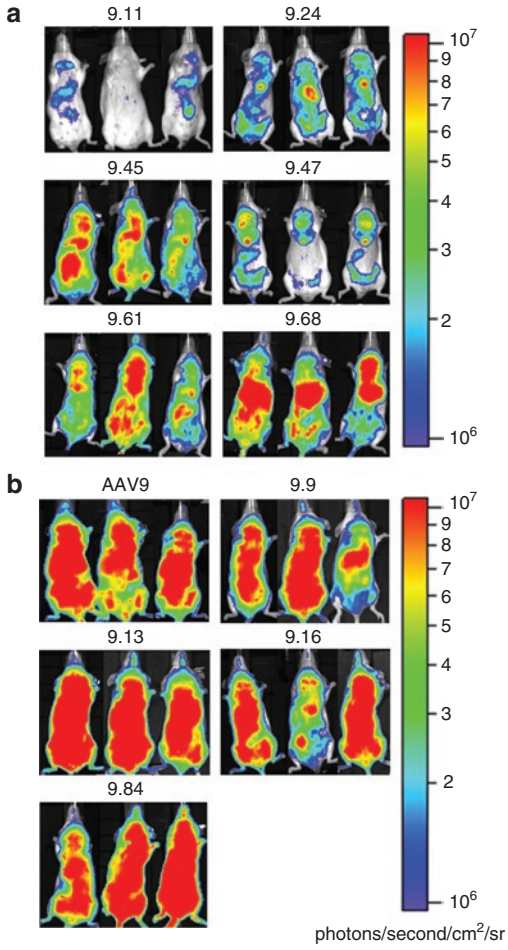

Figure 2 Bioluminescent live animal images at 4 weeks postadministration of vectors packaging the chicken β-actin-luc transgene cassette. Panels of mice treated with adeno-associated virus serotype 9 (AAV9) variants displaying (**a**) altered and (**b**) unaltered transduction profiles relative to parental AAV9 vectors are shown. Images (n = 3 each) were obtained at 1 minute exposure using a Xenogen IVIS Lumina system equipped with a CCD camera. Rainbow scale represents relative light units as determined using the Living Image software.

other variants as demonstrated by the lower heart-to-liver ratio for gene expression (approximately threefold) and vector genome copy number (approximately fivefold) (**Figure 6a,b**). Variants 9.9, 9.16, and 9.84 transduced most tissue types as efficiently as parental AAV9 vectors. The latter subset of AAV9 variants displayed approximately two- to fivefold decrease in transduction levels within the liver and a concomitant decrease in vector genome copy numbers (approximately two- to threefold). Taken together, AAV9.13 and 9.68 were assigned under functional subtype III, while AAV9.9, 9.16 and 9.84 appear to overlap between functional subtypes II and III.

Kinetics of transgene expression and dose–response profile of AAV9.45 is distinct from AAV9

We determined the effects of vector dose and time course of transgene expression on AAV9 and AAV9.45 vectors. As shown in **Figure 4a**, both AAV9 and AAV9.45 demonstrate similar kinetics of transgene expression in the heart. However, in case of liver, transduction levels achieved by AAV9.45 appear to reach

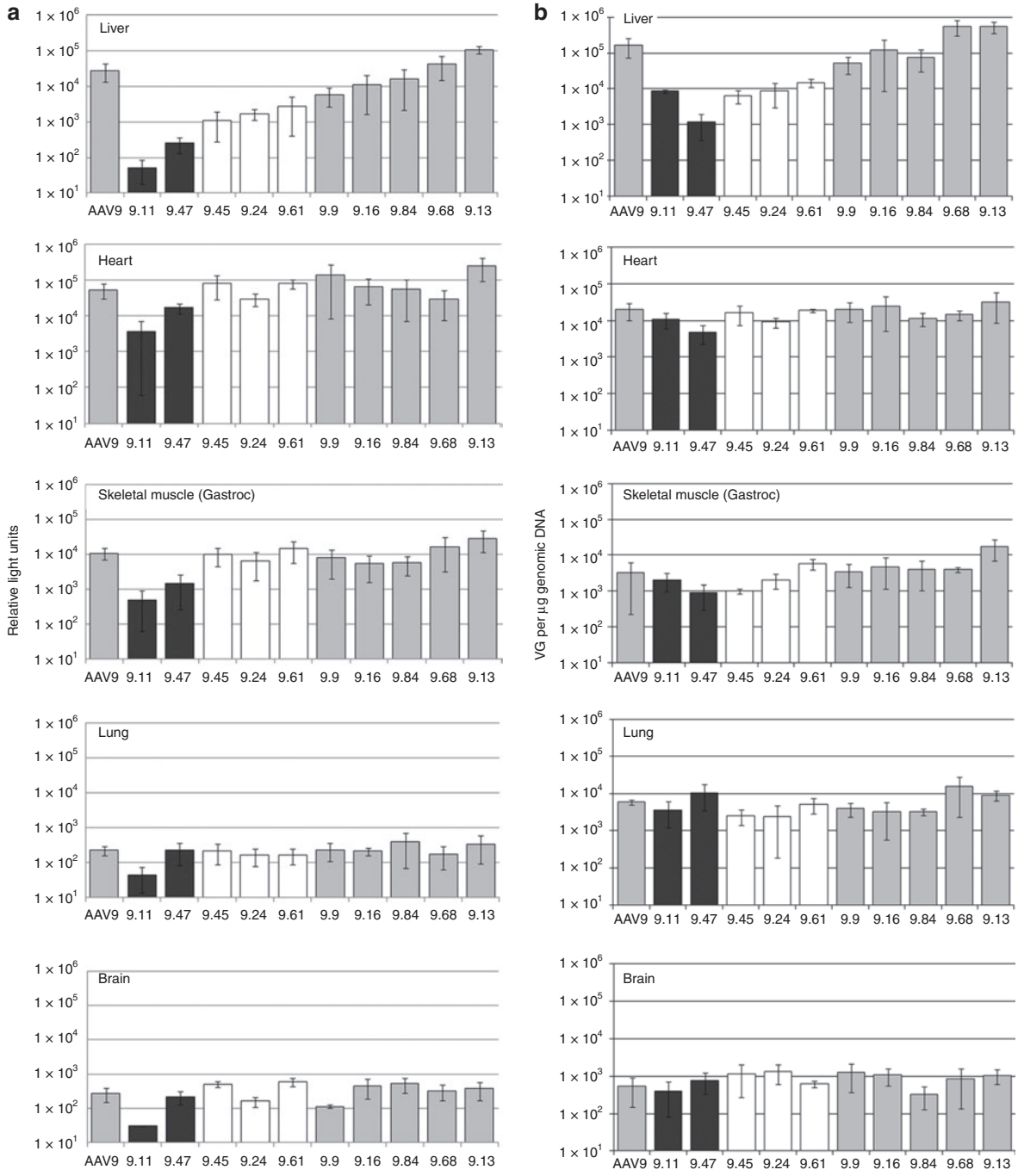

Figure 3 ***In vivo*** **characterization of adeno-associated virus serotype 9 (AAV9) variants.** (**a**) Quantitation of luciferase transgene expression levels and (**b**) vector genome copy numbers at 4 weeks postinjection in different tissue types; heart, liver, skeletal muscle (gastrocnemius), lung, and brain. Defective variants 9.11 and 9.47 (black bars) are categorized under functional subtype I; liver-detargeted variants 9.24, 9.45 and 9.61 (white bars) under functional subtype II; and variants largely similar to AAV9 (gray bars) assigned to functional subtype III. Luciferase expression levels were normalized for total tissue protein concentration is represented as relative light units. Vector genome copy numbers are normalized per µg of genomic DNA. All experiments were carried out in triplicate. Error bars represent standard deviation.

a maximum after 1 week, while AAV9 continues to increase by >1 log unit over 4 weeks (**Figure 4b**). In order to gather further insight into the biology of functional subtype II vectors, we also analyzed the effect of increasing vector dose on transduction efficiency of AAV9 and AAV9.45 following intravenous administration. Although the dose–response profile appears similar between AAV9 and AAV9.45 in heart (**Figure 5a**), the latter displays consistently lower transgene expression (~3- to 45-fold) in comparison with AAV9 in the liver (**Figure 5b**). A potential explanation for this phenomenon is the saturation of peripheral organs with AAV9.45 vectors at high dose resulting in increased uptake within the liver.

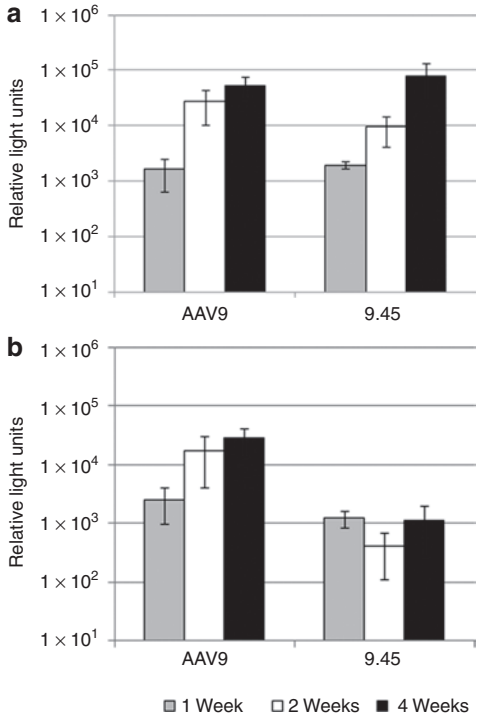

Figure 4 Kinetics of transgene expression. Time course of luciferase transgene expression levels following intravenous administration of adeno-associated virus serotype 9 (AAV9) and AAV9.45 vectors (5×10^{10} vg/mouse) in (**a**) heart and (**b**) liver. Luciferase expression levels determined at 1 week (gray bar), 2 weeks (white bar), and 4 weeks (dark gray bar) were normalized for total tissue protein concentration and data represented as relative light units. All experiments were carried out in triplicate. Error bars represent standard deviation.

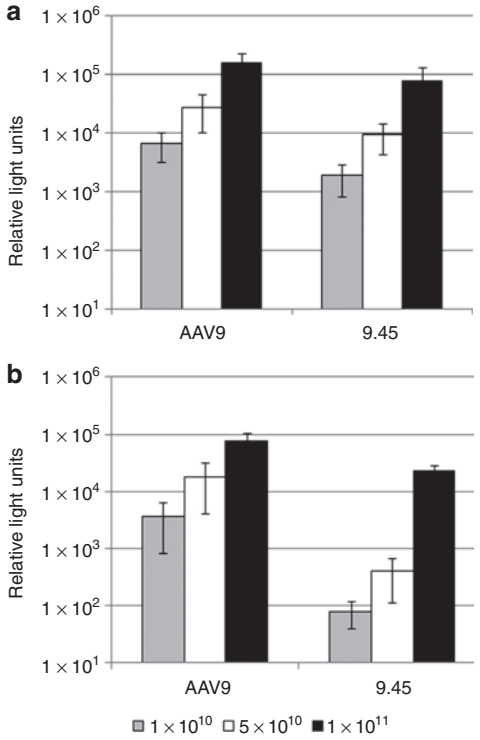

Figure 5 Vector dose–response profile. Effect of vector dose on luciferase transgene expression levels in (**a**) heart and (**b**) liver. Parental adeno-associated virus serotype 9 (AAV9) and AAV9.45 vectors were administered intravenously at low (1×10^{10} vg/mouse), medium (5×10^{10} vg/mouse) and high (1×10^{11} vg/mouse) dose. Luciferase expression assays were carried out to at 2 weeks postadministration and normalized for total tissue protein concentration. Data are represented as relative light units and all experiments were carried out in triplicate. Error bars represent standard deviation.

Variant AAV9.45 is muscle-tropic and efficiently detargeted from the liver

We analyzed the relative tropism of different AAV9 variants for the heart when compared to liver. Briefly, ratios of transgene expression levels as well as vector genome copy numbers in heart and liver tissue lysates were obtained and plotted as shown (**Figure 6a,b**). Variants 9.16, 9.24, 9.9, 9.61, 9.47, 9.11, and 9.45 displayed heart-to-liver ratios for gene expression ~4- to 40-fold higher than parental AAV9 vectors (**Figure 6a**). A concomitant increase in heart-to-liver ratio for vector genome copy number ranging from ~3- to 35-fold was observed (**Figure 6b**). Since 9.11 and 9.47 are classified under defective subtype I, variant AAV9.45 appears to display the highest preference for cardiac transduction. The aforementioned results were further corroborated by histological analysis (**Figure 6c**). Briefly, AAV9 and AAV9.45 vectors packaging a CBA promoter-driven tdTomato reporter transgene were injected through the tail vein, following which liver, cardiac, and skeletal muscle tissue were harvested at 2 weeks postadministration. Fluorescence microscopy of fixed tissue sections confirms that AAV9.45 is cardiac- and skeletal muscle-tropic, while being efficiently detargeted from the liver. In contrast, AAV9 vectors demonstrate robust transduction in all three tissue types as reported previously.[3]

DISCUSSION

Robust systemic transduction following intravenous administration is a hallmark of AAV9 vectors.[3,4,6] Several studies have highlighted the ability of this serotype for efficient cardiac gene transfer as well as the ability to cross the blood brain barrier.[5,28] These attributes make AAV9 a viable candidate for a "top-down" capsid engineering approach that would not only separate individual traits outlined above, but also potentially yield variants with restricted tissue tropisms. Based on aforementioned rationale and guided by structural cues available for other AAV serotypes,[23,24,26,29,30] we generated a randomized AAV9 capsid library with mutations clustered within the VP3 GH loop region which assembles the protrusions that surround the icosahedral threefold axis. We then developed a comprehensive screening approach involving sequence analysis, molecular modeling, and *in vivo* studies to identify variants with novel functional phenotypes.

A critical finding in the current study is the discovery of mutations that result in defective phenotypes. Subtype I includes two variants, AAV9.11 and 9.47 with distinct defects. Mutant 9.11 carries two mutations, T568P and Q590L, which results in a transduction-deficient phenotype. The T568P mutation is buried within the AAV9 trimer (model not shown) and does not appear to impact capsid assembly or packaging efficiency as indicated by viral titers (**Supplementary Table S2**). The Q590L mutation is located within the variable region VIII described by Govindasamy *et al.*[24] Other variants carrying mutations in the AAV9 inner loop region (residues 590–595, VP1 numbering) include AAV9.9 (W595C) and

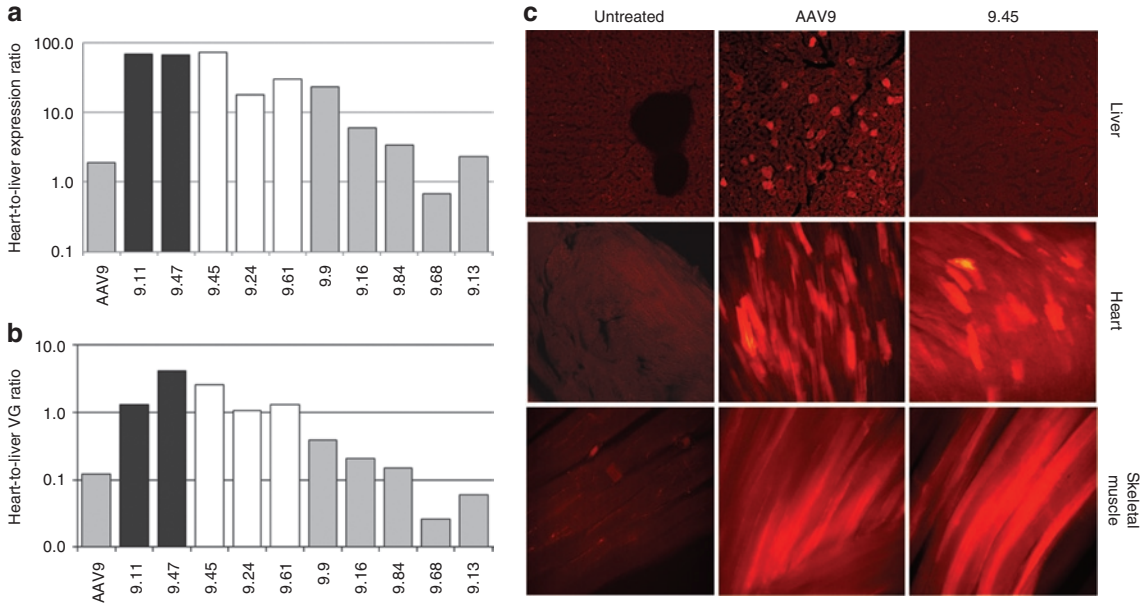

Figure 6 Comparison of transduction profiles of parental adeno-associated virus serotype 9 (AAV9) and variants in heart and liver. (**a**) Heart-to-liver ratios for luciferase expression levels and (**b**) vector genome copy numbers were derived from average values. Variant 9.45 (white bars) demonstrates high heart-to-liver expression and vg ratios and correspondingly high liver-detargeting efficiency. Variant 9.68 displays heart-to-liver ratios lower than parental AAV9 vectors and hence preferential liver transduction. (**c**) Fluorescence micrographs of heart, liver and skeletal muscle (gastrocnemius) tissue sections from mice injected with AAV9 or AAV9.45 vectors packaging the CBA-tdTomato cassette. Images were obtained at ×20 (liver) or ×10 (heart and skeletal muscle) magnification using an Olympus microscope equipped with a Hamamatsu digital camera. Tissue sections from untreated mice are shown as control. All experiments were carried out in duplicate.

AAV9.16 (Q592L), which display a modest decrease in transduction efficiency within the liver in comparison with the parental AAV9. Residues within the corresponding inner loop region on AAV2 have previously been implicated in heparan sulfate binding.[20,21] In corollary, it is likely that mutation of one or more residues within the 590–595 region might alter interaction of AAV9 with its cognate receptor. Variant AAV9.47 displayed a defective biodistribution profile, which in turn adversely affected transduction efficiency. Consistent with this defective profile, AAV9.47 is rapidly eliminated from blood circulation when compared to AAV9, AAV9.45, and AAV9.68 vectors (**Supplementary Figure S1**). One plausible explanation for the latter phenotype is the contribution of G453D and K557E mutations to negatively charged clusters on the AAV9.47 surface (**Figure 1e**), thereby making the capsid prone to rapid blood clearance. A similar decrease in circulation half-life has been observed upon masking positively charged residues or addition of negatively charged moieties to the surface of Qbeta and M13 bacteriophage particles.[31,32]

In the current study, we have identified novel liver-detargeted variants of AAV9 using comprehensive structural analysis and *in vivo* screening. Similar variants of other AAV serotypes developed using rational or combinatorial mutagenesis have been reported in the literature. For instance, altering residues within the heparan sulfate footprint on the AAV2 capsid has yielded liver-detargeted variants.[27,33] Yang *et al.* (2009)[6] recently identified a myocardium-tropic AAVM41 that showed gene transfer efficiency similar to AAV9 in the heart, but 80-fold decrease in gene expression as well as tenfold lower vector genome copy numbers in the liver. Although no contributing domains from AAV9 were observed, the AAVM41 capsid subunit sequence revealed critical domains derived from AAV serotypes 1, 6, and 7 that appear to confer the cardiotropic phenotype. The current study revealed the critical role played by specific amino acid residues in conferring liver tropism to AAV9 vectors. Specifically, subtype II variants 9.24, 9.45, and 9.61 appear to possess mutations (at positions N498 and W503) that cluster within variable region V previously described by Govindasamy *et al.*[24] Further, AAV9.68, a subtype III variant containing a P504T mutation showed preferential liver tropism as demonstrated by a decrease in heart-to-liver transgene expression ratio when compared to AAV9. This region (residues 498–504) is located behind the inner loop residues 590–595 at the threefold symmetry axis (**Figure 1e**) and has previously been shown to play a critical role in transduction for AAV2.[34] In addition, a region including these amino acid residues was also implicated in laminin receptor recognition by AAV8 capsids.[35] Further optimization of AAV9-derived vectors by varying amino acid residues at different positions and/or combining multiple point mutations (e.g., N498, W503, and W595) onto a single AAV9 capsid template could improve liver-detargeting efficiency.

The precise mechanism behind the altered liver tropism of AAV9.45 and other subtype II mutants remains to be determined. Analysis of structural features of different variants in this study suggests that residues 498–504 taken together with the adjacent 590–595 cluster contain key residues (N498, W503, P504, Q590L) that might constitute a partial receptor footprint on the AAV9 capsid (**Figure 7**). Consequently, one potential explanation is that altered affinity for an AAV9 receptor could, in turn, affect liver tropism. It is noteworthy to mention that similar examples have been reported in case of other viruses. For instance, variants of mouse parvovirus (minute virus of mice)[36,37] carrying mutations

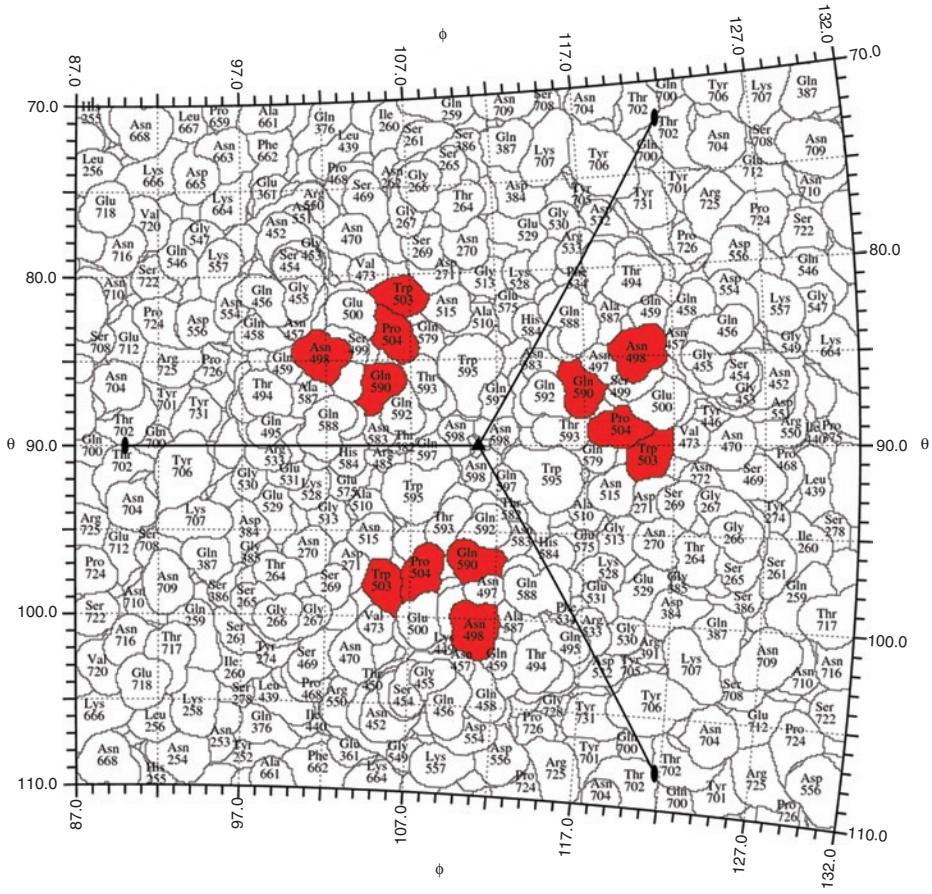

Figure 7 Putative cluster of residues implicated in adeno-associated virus serotype 9 (AAV9) liver tropism. A spherical roadmap projection of surface residues within the AAV9 capsid trimer region was created as described in methods. Key residues, highlighted in red, include N498, W503 (9.45/9.61, 9.24); Q590L (9.11) and P504 (9.68), each derived from mutants categorized under different subtypes. Manipulation of this cluster of residues alters AAV9 liver tropism and might constitute a partial receptor footprint on the AAV9 capsid surface.

that alter receptor binding affinity have also been shown to display altered infectivity and tissue tropism. Another example hinges on the key role played by interactions between the adenovirus capsid hexon protein and vitamin K-dependent coagulation factors in mediating hepatocyte transduction. In this case, alteration of hexon-factor X interactions resulted in liver detargeting of adenoviral vectors.[38] Identification of similar factors such as glycans and/or glycoproteins/glycolipids that dictate AAV9 tissue tropism and analysis of mutant capsid-receptor interactions could provide further insight into the liver-detargeting mechanism.

Liver-detargeted AAV9 variants demonstrate significant potential for gene transfer in the treatment of cardiac and musculoskeletal diseases. Further optimization of liver-detargeted AAV9 vectors with transcriptional targeting elements such as cardiac- or muscle-specific promoters[39,14] or microRNA-122 target sequences[40,41] would allow selective delivery of therapeutic transgenes to heart and/or skeletal muscle.

MATERIALS AND METHODS

Generation of AAV9 capsid library. The AAV9 helper plasmid, pXR9, containing AAV2 *Rep* and AAV9 *Cap* genes was obtained from the University of North Carolina Vector Core. A random plasmid library was generated by subjecting the capsid region encoding amino acids 390 to 627 (VP1 numbering; Genbank: AY530579.1)[42] to error-prone PCR using forward 5′-GGT CGT TCG TCC TTT TAC TGC CTG GAA-3′ and reverse 5′-GCC GTC CGT GTG AGG AAT TTT GGC CCA-3′ primers (Integrated DNA Technologies, Coralville, IA). Cycling was carried out as per manufacturer instructions outlined in the GeneMorph II EZ clone domain mutagenesis kit (Agilent Technologies, Santa Clara, CA). Sequencing of individual clones was carried out by the University of North Carolina Genome Analysis facility and capsid sequences analyzed using VectorNTI software (Invitrogen, Carlsbad, CA).

Molecular modeling studies. Homology models of the VP3 monomer of AAV9 and different variants were generated using the SWISS-MODEL online 3D model building server[43] (http://swissmodel.expasy.org/) with the crystal structure of AAV8 as template (PDB ID: 2QA0).[26] VP3 trimer models were obtained using the online oligomer generator tool in the VIPERdb2 database[44] (http://viperdb.scripps.edu/). Surface rendered depictions of amino acid positions and cartoon models were generated using the program Pymol (The PyMOL Molecular Graphics System, Schrödinger LLC, http://www.pymol.org/). Lastly, "roadmap" projections of the AAV9 capsid surface highlighting different amino acid residues were constructed using the Radial Interpretation of Viral Electron Density Maps program.[45]

Cell lines, plasmids, and viruses. HEK 293 cells were maintained at 37 °C in 5% CO_2 in Dulbecco's modified Eagle's medium supplemented with 10% fetal bovine serum and penicillin-streptomycin-amphotericin B. Parental

and variant pXR9 plasmid stocks were obtained from the randomized library described earlier. The plasmid pXX6-80, containing adenoviral helper genes was obtained from the University of North Carolina vector core. Vector cassettes, pTR-CBA-Luc, containing the CBA promoter-driven luciferase transgene and pTR-CBA-Tom, encoding tdTomato—a red fluorescent protein, were generated by ligating Luc/Tom inserts flanked by BamHI-NotI sites into the pTR-CBA backbone. Parental and variant AAV9 vectors were produced by the triple-transfection method followed by cesium chloride gradient ultracentrifugation and dialysis as described elsewhere.[46] Viral titers were determined by qPCR using a Roche Lightcycler with primers specific for the CBA promoter (forward 5′-CGT CAA TGG GTG GAG TAT TT-3′; reverse 5′-GCG ATG ACT AAT ACG TAG ATG-3′) or Luc transgene region (forward 5′-AAA AGC ACT CTG ATT GAC AAA TAC-3′; reverse 5′-CCT TCG CTT CAA AAA ATG GAA C-3′).

Animal studies. Housing and handling of BALB/c mice used in the current study were carried out in compliance with National Institutes of Health guidelines and approved by Institutional Animal Care and Use Committee at University of North Carolina–Chapel Hill (#09-117). At 8–10 weeks of age, animals were injected via the tail vein with a dose of 5×10^{10} vector genome-containing particles of AAV9 and related variants packaging CBA-luc or CBA-tom vector cassettes. Luciferase expression in animals was imaged at different time intervals using a Xenogen IVIS Lumina imaging system (Caliper Lifesciences, Hopkinton, MA) following intraperitoneal injection of D-luciferin substrate (120 mg/kg; Nanolight, Pinetop, AZ). Bioluminescent image analysis was carried out using the Living Image software.

Quantitation of luciferase expression. The same group of animals utilized for imaging studies, were killed at 4 weeks postinjection and the following organs were collected: brain, heart, lung, liver, and skeletal muscle (gastrocnemius). Approximately 50 mg of each tissue was homogenized in 150 µl of passive lysis buffer (Promega, Madison, WI) using a Tissue lyser II system (Qiagen, Valencia, CA). Tissue lysates were centrifuged at 8,000 rpm for 2 minutes to pellet debris and 50 µl of the supernatant transferred to 96-well plates for luminometric analysis (Promega) using a Victor2 luminometer (Perkin Elmer, Waltham, MA). Total protein concentration in tissue lysates was determined using the Bradford assay (BioRad, Hercules, CA). For monitoring time course of gene expression, AAV9 and AAV9.45 vectors were administered at a dose of 5×10^{10} vg/mouse to three different groups of animals. After being killed at 1, 2, and 4 weeks, heart and liver tissue from each group were processed for quantitation of luciferase transgene expression as described earlier. In order to determine the effect of vector dose on transgene expression level, AAV9 and AAV9.45 vectors were administered at three different doses: low (1×10^{10} vg per mouse), medium (5×10^{10} vg per mouse) and high (1×10^{11} vg per mouse). Animals were killed at 2 weeks postadministration, following which heart and liver tissue were processed further for determination of luciferase transgene expression levels.

Quantitation of vector genomes. Approximately 100 µl of supernatant from tissue lysates obtained as mentioned above was processed using a DNeasy kit (Qiagen) to extract host and vector genomic DNA. Vector genome (Luc) and mouse lamin gene (internal standard) copy numbers were determined from 100 ng of total extracted DNA using qPCR. Vector genome copy numbers in blood were determined at different time intervals following intravenous administration of 1×10^{10} particles of AAV9 and related variants packaging the CBA-luc cassette. At 1, 24, and 48 hours postinjection, 10 µl of whole blood was collected from the tail vein in heparinized capillary tubes (Fisherbrand Hematocrit) and viral DNA quantified by qPCR.

Histological analysis. Two weeks after intravenous administration of 5×10^{10} particles of AAV9 and related variants packaging the CBA-tom cassette, mice were overdosed with intraperitoneal avertin (0.2 ml/10 g of a 1.25% solution) and perfused transcardially with ice-cold phosphate-buffered saline, then freshly prepared 4% paraformaldehyde in phosphate-buffered saline. Heart and liver tissues were then fixed overnight at 4 °C and 40 µm thick sections cut using a Leica vibrating blade microtome. Tissue sections were then imaged using an Olympus fluorescence microscope equipped with a rhodamine filter (emission max: 580 nm) and images collected using a Hamamatsu digital camera.

SUPPLEMENTARY MATERIAL

Figure S1. Blood circulation profiles of adeno-associated virus serotype 9 (AAV9) and representative variants from each functional subtype; AAV9.47 (I), AAV9.45 (II) and AAV9.68 (III).
Table S1. List of variants.
Table S2. Vector genome titers.

ACKNOWLEDGMENTS

We thank Jana Phillips, Kelli Bryant, and Sarah Brown for technical help with animal studies. We also thank Eric Horowitz for constructing the pTR-CBA-Tom cassette. This work was supported by National Institutes of Health (NIH) grant HL089221, ARRA funds HL089221-S1/S2 and a National Scientist Development Grant from the American Heart Association awarded to A.A.; and NIH grant GM082926 to M.A.-M. The authors declared no conflict of interest.

REFERENCES

1. Herzog, RW, Cao, O and Srivastava, A (2010). Two decades of clinical gene therapy–success is finally mounting. *Discov Med* **9**: 105–111.
2. Mitchell, AM, Nicolson, SC, Warischalk, JK and Samulski, RJ (2010). AAV's anatomy: roadmap for optimizing vectors for translational success. *Curr Gene Ther* **10**: 319–340.
3. Zincarelli, C, Soltys, S, Rengo, G and Rabinowitz, JE (2008). Analysis of AAV serotypes 1-9 mediated gene expression and tropism in mice after systemic injection. *Mol Ther* **16**: 1073–1080.
4. Inagaki, K, Fuess, S, Storm, TA, Gibson, GA, Mctiernan, CF, Kay, MA *et al.* (2006). Robust systemic transduction with AAV9 vectors in mice: efficient global cardiac gene transfer superior to that of AAV8. *Mol Ther* **14**: 45–53.
5. Pacak, CA, Mah, CS, Thattaliyath, BD, Conlon, TJ, Lewis, MA, Cloutier, DE *et al.* (2006). Recombinant adeno-associated virus serotype 9 leads to preferential cardiac transduction *in vivo*. *Circ Res* **99**: e3–e9.
6. Yang, L, Jiang, J, Drouin, LM, Agbandje-McKenna, M, Chen, C, Qiao, C *et al.* (2009). A myocardium tropic adeno-associated virus (AAV) evolved by DNA shuffling and *in vivo* selection. *Proc Natl Acad Sci USA* **106**: 3946–3951.
7. Foust, KD, Nurre, E, Montgomery, CL, Hernandez, A, Chan, CM and Kaspar, BK (2009). Intravascular AAV9 preferentially targets neonatal neurons and adult astrocytes. *Nat Biotechnol* **27**: 59–65.
8. Kornegay, JN, Li, J, Bogan, JR, Bogan, DJ, Chen, C, Zheng, H *et al.* (2010). Widespread muscle expression of an AAV9 human mini-dystrophin vector after intravenous injection in neonatal dystrophin-deficient dogs. *Mol Ther* **18**: 1501–1508.
9. Lipskaia, L, Chemaly, ER, Hadri, L, Lompre, AM and Hajjar, RJ (2010). Sarcoplasmic reticulum Ca(2+) ATPase as a therapeutic target for heart failure. *Expert Opin Biol Ther* **10**: 29–41.
10. Hasbrouck, NC and High, KA (2008). AAV-mediated gene transfer for the treatment of hemophilia B: problems and prospects. *Gene Ther* **15**: 870–875.
11. Brantly, ML, Chulay, JD, Wang, L, Mueller, C, Humphries, M, Spencer, LT *et al.* (2009). Sustained transgene expression despite T lymphocyte responses in a clinical trial of rAAV1-AAT gene therapy. *Proc Natl Acad Sci USA* **106**: 16363–16368.
12. Halbert, CL, Madtes, DK, Vaughan, AE, Wang, Z, Storb, R, Tapscott, SJ *et al.* (2010). Expression of human alpha1-antitrypsin in mice and dogs following AAV6 vector-mediated gene transfer to the lungs. *Mol Ther* **18**: 1165–1172.
13. Salva, MZ, Himeda, CL, Tai, PW, Nishiuchi, E, Gregorevic, P, Allen, JM *et al.* (2007). Design of tissue-specific regulatory cassettes for high-level rAAV-mediated expression in skeletal and cardiac muscle. *Mol Ther* **15**: 320–329.
14. Wang, B, Li, J, Fu, FH, Chen, C, Zhu, X, Zhou, L *et al.* (2008). Construction and analysis of compact muscle-specific promoters for AAV vectors. *Gene Ther* **15**: 1489–1499.
15. Brown, BD and Naldini, L (2009). Exploiting and antagonizing microRNA regulation for therapeutic and experimental applications. *Nat Rev Genet* **10**: 578–585.
16. Michelfelder, S, Kohlschütter, J, Skorupa, A, Pfennings, S, Müller, O, Kleinschmidt, JA *et al.* (2009). Successful expansion but not complete restriction of tropism of adeno-associated virus by *in vivo* biopanning of random virus display peptide libraries. *PLoS ONE* **4**: e5122.
17. Ying, Y, Müller, OJ, Goehringer, C, Leuchs, B, Trepel, M, Katus, HA *et al.* (2010). Heart-targeted adeno-associated viral vectors selected by *in vivo* biopanning of a random viral display peptide library. *Gene Ther* **17**: 980–990.
18. Excoffon, KJ, Koerber, JT, Dickey, DD, Murtha, M, Keshavjee, S, Kaspar, BK *et al.* (2009). Directed evolution of adeno-associated virus to an infectious respiratory virus. *Proc Natl Acad Sci USA* **106**: 3865–3870.
19. Koerber, JT, Klimczak, R, Jang, JH, Dalkara, D, Flannery, JG and Schaffer, DV (2009). Molecular evolution of adeno-associated virus for enhanced glial gene delivery. *Mol Ther* **17**: 2088–2095.
20. Opie, SR, Warrington, KH Jr, Agbandje-McKenna, M, Zolotukhin, S and Muzyczka, N (2003). Identification of amino acid residues in the capsid proteins of adeno-

associated virus type 2 that contribute to heparan sulfate proteoglycan binding. *J Virol* **77**: 6995–7006.
21. Kern, A, Schmidt, K, Leder, C, Müller, OJ, Wobus, CE, Bettinger, K *et al.* (2003). Identification of a heparin-binding motif on adeno-associated virus type 2 capsids. *J Virol* **77**: 11072–11081.
22. Asokan, A, Hamra, JB, Govindasamy, L, Agbandje-McKenna, M and Samulski, RJ (2006). Adeno-associated virus type 2 contains an integrin alpha5beta1 binding domain essential for viral cell entry. *J Virol* **80**: 8961–8969.
23. Xie, Q, Bu, W, Bhatia, S, Hare, J, Somasundaram, T, Azzi, A *et al.* (2002). The atomic structure of adeno-associated virus (AAV-2), a vector for human gene therapy. *Proc Natl Acad Sci USA* **99**: 10405–10410.
24. Govindasamy, L, Padron, E, McKenna, R, Muzyczka, N, Kaludov, N, Chiorini, JA *et al.* (2006). Structurally mapping the diverse phenotype of adeno-associated virus serotype 4. *J Virol* **80**: 11556–11570.
25. Wu, Z, Asokan, A, Grieger, JC, Govindasamy, L, Agbandje-McKenna, M and Samulski, RJ (2006). Single amino acid changes can influence titer, heparin binding, and tissue tropism in different adeno-associated virus serotypes. *J Virol* **80**: 11393–11397.
26. Nam, HJ, Lane, MD, Padron, E, Gurda, B, McKenna, R, Kohlbrenner, E *et al.* (2007). Structure of adeno-associated virus serotype 8, a gene therapy vector. *J Virol* **81**: 12260–12271.
27. Asokan, A, Conway, JC, Phillips, JL, Li, C, Hegge, J, Sinnott, R *et al.* (2010). Reengineering a receptor footprint of adeno-associated virus enables selective and systemic gene transfer to muscle. *Nat Biotechnol* **28**: 79–82.
28. Bish, LT, Morine, K, Sleeper, MM, Sanmiguel, J, Wu, D, Gao, G *et al.* (2008). Adeno-associated virus (AAV) serotype 9 provides global cardiac gene transfer superior to AAV1, AAV6, AAV7, and AAV8 in the mouse and rat. *Hum Gene Ther* **19**: 1359–1368.
29. Levy, HC, Bowman, VD, Govindasamy, L, McKenna, R, Nash, K, Warrington, K *et al.* (2009). Heparin binding induces conformational changes in Adeno-associated virus serotype 2. *J Struct Biol* **165**: 146–156.
30. Lerch, TF, Xie, Q and Chapman, MS (2010). The structure of adeno-associated virus serotype 3B (AAV-3B): insights into receptor binding and immune evasion. *Virology* **403**: 26–36.
31. Molenaar, TJ, Michon, I, de Haas, SA, van Berkel, TJ, Kuiper, J and Biessen, EA (2002). Uptake and processing of modified bacteriophage M13 in mice: implications for phage display. *Virology* **293**: 182–191.
32. Prasuhn, DE Jr, Singh, P, Strable, E, Brown, S, Manchester, M and Finn, MG (2008). Plasma clearance of bacteriophage Qbeta particles as a function of surface charge. *J Am Chem Soc* **130**: 1328–1334.
33. Michelfelder, S and Trepel, M (2009). Adeno-associated viral vectors and their redirection to cell-type specific receptors. *Adv Genet* **67**: 29–60.
34. Lochrie, MA, Tatsuno, GP, Christie, B, McDonnell, JW, Zhou, S, Surosky, R *et al.* (2006). Mutations on the external surfaces of adeno-associated virus type 2 capsids that affect transduction and neutralization. *J Virol* **80**: 821–834.
35. Akache, B, Grimm, D, Pandey, K, Yant, SR, Xu, H and Kay, MA (2006). The 37/67-kilodalton laminin receptor is a receptor for adeno-associated virus serotypes 8, 2, 3, and 9. *J Virol* **80**: 9831–9836.
36. Rubio, MP, López-Bueno, A and Almendral, JM (2005). Virulent variants emerging in mice infected with the apathogenic prototype strain of the parvovirus minute virus of mice exhibit a capsid with low avidity for a primary receptor. *J Virol* **79**: 11280–11290.
37. Nam, HJ, Gurda-Whitaker, B, Gan, WY, Ilaria, S, McKenna, R, Mehta, P *et al.* (2006). Identification of the sialic acid structures recognized by minute virus of mice and the role of binding affinity in virulence adaptation. *J Biol Chem* **281**: 25670–25677.
38. Kalyuzhniy, O, Di Paolo, NC, Silvestry, M, Hofherr, SE, Barry, MA, Stewart, PL *et al.* (2008). Adenovirus serotype 5 hexon is critical for virus infection of hepatocytes *in vivo*. *Proc Natl Acad Sci USA* **105**: 5483–5488.
39. Boecker, W, Bernecker, OY, Wu, JC, Zhu, X, Sawa, T, Grazette, L *et al.* (2004). Cardiac-specific gene expression facilitated by an enhanced myosin light chain promoter. *Mol Imaging* **3**: 69–75.
40. Qiao, C, Yuan, Z, Li, J, He, B, Zheng, H, Mayer, C,*et al.* (2010). Liver-specific microRNA-122 target sequences incorporated in AAV vectors efficiently inhibits transgene expression in the liver. *Gene Ther* (epub ahead of print).
41. Geisler, A, Jungmann, A, Kurreck, J, Poller, W, Katus, HA, Vetter, R *et al.* (2011). microRNA122-regulated transgene expression increases specificity of cardiac gene transfer upon intravenous delivery of AAV9 vectors. *Gene Ther* **18**: 199–209.
42. Gao, G, Vandenberghe, LH, Alvira, MR, Lu, Y, Calcedo, R, Zhou, X *et al.* (2004). Clades of Adeno-associated viruses are widely disseminated in human tissues. *J Virol* **78**: 6381–6388.
43. Arnold, K, Bordoli, L, Kopp, J and Schwede, T (2006). The SWISS-MODEL workspace: a web-based environment for protein structure homology modelling. *Bioinformatics* **22**: 195–201.
44. Carrillo-Tripp, M, Shepherd, CM, Borelli, IA, Venkataraman, S, Lander, G, Natarajan, P *et al.* (2009). VIPERdb2: an enhanced and web API enabled relational database for structural virology. *Nucleic Acids Res* **37**(Database issue): D436–D442.
45. Xiao, C and Rossmann, MG (2007). Interpretation of electron density with stereographic roadmap projections. *J Struct Biol* **158**: 182–187.
46. Grieger, JC, Choi, VW and Samulski, RJ (2006). Production and characterization of adeno-associated viral vectors. *Nat Protoc* **1**: 1412–1428.